Adaptive Interpolation Based on Pólya Frequency Functions

Luc Knockaert, *Senior Member, IEEE*, Daniël De Zutter, *Fellow, IEEE*, and Tom Dhaene, *Senior Member, IEEE*

***Abstract*—Translation-invariant interpolation of frequency domain functions by means of Fourier transforms of Pólya frequency functions, which belong to the Bochner class of interpolation kernels, is presented. For the implementation, we use an adaptive interpolation process which is a variant of the recently introduced adaptive residual subsampling method. Moreover, it is shown that adaptive residual subsampling with Pólya interpolation kernels is an excellent preprocessing interface when used in conjunction with the well-known vector fitting (VF) rational modeling algorithm.**

***Index Terms*—Adaptive interpolation, causality, quasi-rational modeling, radial basis functions, rational modeling.**

I. Introduction

RADIAL basis functions (RBF) constitute a powerful tool for translation-invariant interpolation on nonuniformly sampled data. They are used extensively for scattered data interpolation [1], medical imaging [2] and are also frequently applied to neural networks [3]. As a consequence of Bochner's theorem [4], the most salient feature of radial basis functions is that the interpolation process they induce is always well-conditioned. In general multivariate interpolation with radial basis functions [1], [5], Bochner's theorem and the related Schoenberg theorem [6], are the main theoretical tools instrumental in the selection of well-conditioned positive definite interpolation kernels [7].

In this paper, we first discuss the translation-invariant interpolation of frequency domain functions by means of Fourier transforms of Pólya frequency functions [8]–[10], which although belonging to the Bochner class of interpolation kernels, are not necessarily RBFs. We select two pertinent Pólya interpolation kernels, a rational noncausal radial kernel, and a new quasi-rational quasi-causal kernel. This results in rational, respectively, quasi-rational approximations of the input frequency domain function. For the practical implementation, we use a local adaptive interpolation process which is a variant of the recently introduced adaptive residual subsampling (ARS) method [11].

Manuscript received April 19, 2007; revised February 26, 2008. Current version published September 17, 2008. The associate editor coordinating the review of this manuscript and approving it for publication was Dr. Thierry Blu. This work was supported by a grant from the Research Foundation-Flanders (FWO-Vlaanderen).

The authors are with the Interdisciplinary Institute for Broadband Technology (IBBT) and the Department of Information Technology, Ghent University, B-9050 Ghent, Belgium (e-mail: luc.knockaert@intec.ugent.be).

Color versions of one or more of the figures in this paper are available online at http://ieeexplore.ieee.org.

Digital Object Identifier 10.1109/TSP.2008.923200

Second, we deal with the rational approximation and interpolation problem, which arises naturally in signal processing [12], numerical analysis [13] and system identification [14]. In that context, the vector fitting (VF) algorithm [15], which was shown [16] to be a modified version of the Sanathanan-Koerner [17], [14] approach, has grown very popular in the Applied Mathematics and Engineering communities. For instance, VF has its own website which references 36 papers on the subject.[1]

In this paper, we show that ARS with the Pólya interpolation kernels introduced earlier provides an excellent preprocessing interface when used in conjunction with the VF algorithm for obtaining rational models over a given frequency range. The reason for this is that ARS automatically generates the sampling nodes (unspecified and presumed equispaced by default in VF) and the starting poles (chosen more or less heuristically in VF [15]) which are required for the initialization of the VF algorithm. This results in a composite algorithm, performing the sampling and modelling of the input frequency domain function in a fully automatic way. Of course, ARS preprocessing requires the availability of an analytic formula (an oracle run in the background) for the frequency domain function which we want to approximate. If only discrete sampled-data are available, which is often the case in practice, the oracle might consist of an interpolatory engine (linear, spline, etc.) mapping the discrete samples on a "smooth" analytic formula, but this is not exhaustive.

Finally, three pertinent examples, one analytical causal, one analytical noncausal, and one real-world (a bandstop filter from EM-simulations), show the versatility and strength of the proposed method.

II. Preliminaries

Definition 1: A complex-valued continuous function $h(x)$ is called positive definite on $\mathbb{R}^d$ if

$$\sum_{j=1}^{N}\sum_{k=1}^{N} c_j\overline{c_k}h(x_j - x_k) \geq 0 \tag{1}$$

for any N pairwise different points $x_1,\ldots,x_N \in \mathbb{R}^d$, and $c = (c_1,\ldots,c_N)^T \in \mathbb{C}^N$. The function $h(x)$ is called strictly positive definite on $\mathbb{R}^d$ if the only vector c that turns (1) into an equality is the zero vector.

Definition 2: A complex-valued function $h(x)$ is called radial if $h(x) = F(\|x\|)$ where $\|x\|$ is the Euclidean norm in $\mathbb{R}^d$.

[1]Website available online at http://www.energy.sintef.no/produkt/VECTFIT/index.asp. Searching for the keyword "Vector Fitting"' on Google Scholar also yields 323 undisputable hits concerning the VF algorithm and its variants.

Theorem 1 (Bochner): A complex-valued function $h(x)$ is positive definite on $\mathbb{R}^d$ if and only if it is the Fourier transform of a finite nonnegative Borel measure μ on $\mathbb{R}^d$, i.e.,

$$h(x) = \int_{\mathbb{R}^d} e^{-ix\cdot y} d\mu(y) \tag{2}$$

Moreover, let μ be a nonnegative finite Borel measure on $\mathbb{R}^d$ whose carrier is not a set of Lebesgue measure zero. Then the Fourier transform (2) is strictly positive definite on $\mathbb{R}^d$.

Proof: See [4]. Note that $d\mu(y)$ in (2) may be equivalently replaced by $\nu(y)\,dy$, where $\nu(y) \geq 0$ is the Radon–Nikodym derivative $d\mu(y)/dy$.

Theorem 2 (Schoenberg): A continuous function $h(x) = F(\|x\|)$ is positive definite and radial on $\mathbb{R}^d$ for all $d = 1, 2, 3, \ldots$ if and only if it is of the form

$$F(r) = \int_0^\infty e^{-r^2t^2}\, d\mu(t) \tag{3}$$

where μ is a finite nonnegative Borel measure on $[0, \infty)$.

Proof: See [6].

Definition 3: A nonnegative measurable function $\Lambda(x)$ on $\mathbb{R}$ satisfying $0 < \int_{\mathbb{R}} \Lambda(x)\,dx < \infty$ is called a Pólya frequency function provided it satisfies the following condition : for every two sets of strictly increasing numbers

$$x_1 < x_2 < \cdots < x_n \quad y_1 < y_2 < \cdots < y_n \quad n = 1, 2, \cdots \tag{4}$$

we have

$$\det\{\Lambda(x_i - y_j)\}_{1,n} \geq 0. \tag{5}$$

Theorem 3 (Schoenberg): The double-sided Laplace transform of a Pólya frequency function $\Lambda(x)$ converges in a vertical strip containing the origin, and can there be written as

$$\int_{-\infty}^{\infty} e^{-sx}\Lambda(x)\,dx = \frac{1}{\Psi(s)} \tag{6}$$

where $\Psi(s)$ is an entire function of the form

$$\Psi(s) = Ce^{-\gamma s^2 - \delta_0 s} \prod_{m=1}^{\infty} (1 + s\delta_m)e^{-s\delta_m} \tag{7}$$

$$C > 0, \quad \gamma \geq 0, \quad \delta_m \in \mathbb{R}, \quad 0 < \gamma + \sum_{m=1}^{\infty} \delta_m^2 < \infty. \tag{8}$$

Moreover, when $\gamma > 0$, the function $\Lambda(x) > 0$ is of class $C^\infty(\mathbb{R})$ such that the derivatives $\Lambda^{(n)}(x)$ have exactly n simple real zeros for all values of n.

Proof: See [8]–[10].

Definition 4: A function $Q(z)$ is called quasi-rational if it can be written as $Q(z) = R(z)E(z)$, where $R(z)$ is a rational function and $E(z)$ is an entire function (not a polynomial). The quasi-rational function $Q(z)$ is stable whenever the rational function $R(z)$ is stable, i.e., all its poles are in the open left half-plane.

A very interesting, very simple Corollary of Theorem 3 (in fact it follows from its converse, see [9]) is that there exist Pólya frequency functions $\Lambda(x)$ such that their double-sided Laplace transform is a quasi-rational function. This can e.g., be seen by taking $\delta_m = 0$ for $m > M_0 \geq 1$ in (8), yielding

$$\int_{-\infty}^{\infty} e^{-sx}\Lambda(x)\,dx = \frac{1}{C}\, e^{\gamma s^2 + \sum_{m=0}^{M_0} \delta_m s} \prod_{m=1}^{M_0} \frac{1}{1 + s\delta_m}. \tag{9}$$

Definition 5: The causality index $\mathcal{C}_1(h)$ of a $L_1(\mathbb{R})$ function $h(x)$ with inverse Fourier transform

$$\Lambda(y) = \frac{1}{2\pi} \int_{-\infty}^{\infty} e^{ixy} h(x)\,dx \tag{10}$$

is defined as

$$\mathcal{C}_1(h) = \frac{\int_0^\infty |\Lambda(y)|\,dy}{\int_{-\infty}^\infty |\Lambda(y)|\,dy} \tag{11}$$

provided, of course, that $\int_{-\infty}^\infty |\Lambda(y)|\,dy > 0$. It is easy to prove that $0 \leq \mathcal{C}_1(h) \leq 1$ and

$$\mathcal{C}_1(\alpha h(\beta x + \gamma)) = \frac{1}{2} + \operatorname{sgn}\beta \left(\mathcal{C}_1(h) - \frac{1}{2}\right)$$
$$\alpha \in \mathbb{C}\backslash\{0\} \quad \beta \in \mathbb{R}\backslash\{0\} \quad \gamma \in \mathbb{R}. \tag{12}$$

Theorem 4: Let

$$h_k(x) = \int_{-\infty}^{\infty} e^{-ixy}\Lambda_k(y)\,dy \quad k = 1, \ldots, M \tag{13}$$

with all $\Lambda_k(y) \geq 0$ and $0 < \int_{-\infty}^\infty \Lambda_k(y) < \infty$. Then

$$\min_k \{\mathcal{C}_1(h_k)\} \leq \mathcal{C}_1\left(\sum_{k=1}^M h_k\right) \leq \max_k \{\mathcal{C}_1(h_k)\}. \tag{14}$$

Proof: The premises imply that

$$\mathcal{C}_1\left(\sum_{k=1}^M h_k\right) = \frac{\sum_{k=1}^M \mathcal{C}_1(h_k) \int_{-\infty}^\infty \Lambda_k(y)\,dy}{\sum_{k=1}^M \int_{-\infty}^\infty \Lambda_k(y)\,dy}. \tag{15}$$

This can be written as

$$\mathcal{C}_1\left(\sum_{k=1}^M h_k\right) = \sum_{k=1}^M p_k\, \mathcal{C}_1(h_k) \quad p_k \geq 0 \quad \sum_{k=1}^M p_k = 1 \tag{16}$$

and the result follows. □

For a function $h(x)$ satisfying the premises of Theorem 4, in other words, a function $h(x)$ that is the Fourier transform of a nonnegative function, it can be shown that the following explicit expression for the causality index holds:

$$\mathcal{C}_1(h) = \frac{1}{2} - \frac{1}{\pi h(0)} \int_0^\infty \frac{\Im h(x)}{x}\,dx. \tag{17}$$

III. Translation Invariant Interpolation

The basic problem in approximating a given frequency domain response $H(\omega)$ over a certain frequency range is to construct an approximation to data specified at N distinct

points $\omega_1, \ldots, \omega_N$ in $\mathbb{R}$. A simple solution consists in choosing N functions and then looking for the unique combination of these functions which interpolates the data at the given points. For this process to be successful, the set of functions chosen must be linearly independent over the set of interpolation points $\omega_1, \ldots, \omega_N$. If the functions are $u_1(\omega), \ldots, u_N(\omega)$, then the interpolation problem admits a solution provided the interpolation matrix $A_{i,j} = u_j(\omega_i)$ is invertible and not too ill-conditioned. In translation invariant interpolation we consider $u_k(\omega) = h(\omega - \omega_k)$, where $h(\omega)$, called the interpolation kernel, is strictly positive definite on $\mathbb{R}$. By Definition 1 this implies that the interpolation matrix $A_{i,j} = h(\omega_i - \omega_j)$ is invertible. By Theorem 1, we therefore require that

$$h(\omega) = \int_{\mathbb{R}} e^{-i\omega x} d\mu(x) \tag{18}$$

where μ is a nonnegative finite Borel measure on $\mathbb{R}$ whose carrier is not a set of Lebesgue measure zero. This will certainly be the case when the Radon–Nikodym derivative $d\mu(x)/dx = \Lambda(x)$ is a Pólya frequency function. This is what we will suppose throughout the sequel.

A. Rational Noncausal Radial Interpolation Kernel

The simplest even rational function $1/\Psi(s)$ in (9) is obtained for $M_0 = 2$ and $C = 1, \gamma = \delta_0 = 0$, and $0 < c = \delta_1 = -\delta_2$. In that case, $\Psi(s) = 1 - c^2 s^2$, and the interpolation kernel is

$$h(\omega) = \frac{1}{\Psi(i\omega)} = \frac{1}{1 + c^2\omega^2} = \int_{-\infty}^{\infty} e^{-i\omega x} \Lambda(x)\, dx \tag{19}$$

where

$$\Lambda(x) = \frac{1}{2c} \exp\left(-\frac{|x|}{c}\right) \tag{20}$$

is the Pólya frequency function. Note that, by Theorem 2, the function $h(\omega)$ is a strictly positive definite radial function with Borel measure $\mu(t) = 1 - e^{-t^2/c^2}$. It is also clear that the causality index $\mathcal{C}_1(h) = (1/2)$. The poles of a translate $h(\omega - \omega_0)$ in the Laplace domain are $s = i\omega_0 \pm 1/c$. Hence, we conclude that the kernel (19) is a well-conditioned rational radial, but noncausal and nonstable interpolation kernel.

B. Quasi-Rational Quasi-Causal Interpolation Kernel

The simplest causal stable rational function $1/\Psi(s)$ in (9) is obtained for $M_0 = 1$ and $C = 1, \gamma = 0$ and $0 < c = \delta_1 = -\delta_0$. In that case, $\Psi(s) = 1 + cs$, and the interpolation kernel is

$$h(\omega) = \frac{1}{\Psi(i\omega)} = \frac{1}{1 + i\omega c} = \int_{-\infty}^{\infty} e^{-i\omega x} \Lambda(x)\, dx \tag{21}$$

with Pólya frequency function

$$\Lambda(x) = \frac{1}{c} \exp\left(-\frac{x}{c}\right) \Upsilon(x) \tag{22}$$

where $\Upsilon(x)$ is the Heaviside unit step function. The poles of a translate $h(\omega - \omega_0)$ in the Laplace domain are $s = i\omega_0 - 1/c$. Hence, the kernel (21) is a causal (causality index 1) and stable interpolation kernel. Unfortunately, Theorem 1 indicates (see also [7]) that this kernel will be ill-conditioned, since $\Lambda(x) = 0$ on the negative reals. We can remedy this by taking a positive value for γ. In that case, $\Psi(s) = (1 + cs)e^{-\gamma s^2}$, and the interpolation kernel is

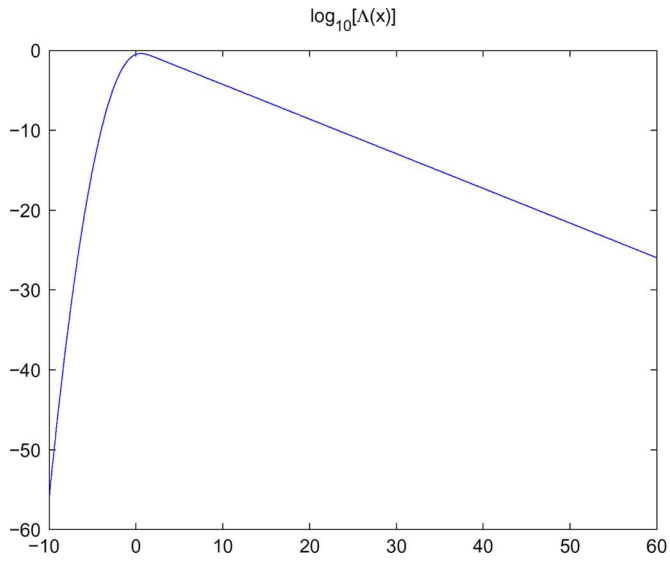

Fig. 1. Logarithm of the quasi-rational quasi-causal Pólya frequency function.

$$h(\omega) = \frac{1}{\Psi(i\omega)} = \frac{e^{-\gamma\omega^2}}{1 + ic\omega} = \int_{-\infty}^{\infty} e^{-i\omega x} \Lambda(x)\, dx \tag{23}$$

with Pólya frequency function

$$\Lambda(x) = \frac{1}{2c} \exp\left(\frac{\gamma - cx}{c^2}\right) \operatorname{erfc}\left(\frac{2\gamma - cx}{2c\sqrt{\gamma}}\right) \tag{24}$$

where $\operatorname{erfc}(\cdot)$ is the complementary error function. The Pólya frequency function (24) is an entire function for $\gamma > 0$, which is always positive in $-\infty < x < \infty$, and, hence, the interpolation kernel (23) is better conditioned than the interpolation kernel (21). A typical plot of the logarithm of $\Lambda(x)$ for $c = 1$ and $\gamma = 0.2$ is shown in Fig. 1. The causality index of $h(\omega)$ can be calculated as

$$\mathcal{C}_1(h) = \frac{1}{2}\left[1 + \exp\left(\frac{\gamma}{c^2}\right) \operatorname{erfc}\left(\frac{\sqrt{\gamma}}{c}\right)\right]. \tag{25}$$

We can fix the causality index by putting $\gamma = \kappa c^2$, with causality parameter $\kappa > 0$, which redefines the interpolation kernel as

$$h(\omega) = \frac{e^{-\kappa c^2 \omega^2}}{1 + ic\omega} \tag{26}$$

with causality index

$$\mathcal{C}_1(h) = \xi(\kappa) \stackrel{\text{def}}{=} \frac{1}{2}\left[1 + \exp(\kappa)\operatorname{erfc}(\sqrt{\kappa})\right]. \tag{27}$$

The function $\xi(\kappa)$ defined in (27) is strictly decreasing with $\xi(0) = 1$ and $\xi(\infty) = (1/2)$. The poles of a translate $h(\omega - \omega_0)$ in the Laplace domain remain $s = i\omega_0 - 1/c$. Hence we conclude that the kernel (26) is a well-conditioned quasi-rational, quasi-causal (for κ sufficiently small) and stable interpolation kernel.

IV. Adaptive Residual Subsampling Interpolation

As we have seen previously, the task in translation-invariant interpolation is to approximate a given function $H(\omega)$ as

$$H(\omega) = \sum_{j=1}^{N} d_j h(\omega - \omega_j). \tag{28}$$

This leads to the system of linear equations

$$Ad = \eta \tag{29}$$

where the interpolation matrix is $A_{i,j} = h(\omega_i - \omega_j)$ and $\eta_i = H(\omega_i)$. In the interpolation kernels analyzed in the previous section, the kernel depends on an additional free multiplicative shape parameter c, i.e., $h(\omega) = \phi(c\omega)$, where we have two possible choices for $\phi(\omega)$, namely

$$\phi(\omega) = \frac{1}{1+\omega^2} \tag{30}$$

$$\phi(\omega) = \frac{e^{-\kappa\omega^2}}{1+i\omega}. \tag{31}$$

This leads to the more involved approximation

$$H(\omega) = \sum_{j=1}^{N} d_j \phi(c_j(\omega - \omega_j)) \tag{32}$$

with interpolation matrix $A_{i,j} = \phi(c_j(\omega_i - \omega_j))$. Naturally, one wants the interpolation error

$$e(\omega) = H(\omega) - \sum_{j=1}^{N} d_j \phi(c_j(\omega - \omega_j)) \tag{33}$$

to be as small as possible (with respect to a given threshold) over the whole frequency range $[\omega_1, \omega_N]$. The interpolation error, although zero at the nodes ω_i, can still be substantial in each of the open intervals (ω_i, ω_{i+1}), and hence the interpolation process must be accomplished adaptively in order to achieve an overall uniformly small interpolation error. We follow the approach advocated in [11]. The shape parameters are chosen as

$$c_1 = \frac{\alpha}{\omega_2 - \omega_1} \quad c_N = \frac{\alpha}{\omega_N - \omega_{N-1}}$$
$$c_j = \min\left(\frac{\alpha}{\omega_j - \omega_{j-1}}, \frac{\alpha}{\omega_{j+1} - \omega_j}\right) \quad j = 2 \ldots N-1 \tag{34}$$

where the parameter α is chosen as

$$\alpha = \frac{|\phi(0)| + |\phi(1)|}{2|\phi(0)|}. \tag{35}$$

The ARS method [11] then proceeds as follows. First, an initial mesh using N_0 (in the examples in the sequel we always take $N_0 = 20$) equally spaced nodes is generated and the interpolation approximation of the function is constructed. Next, the interpolation error at the midpoints between the nodes is computed. Midpoints at which the error exceeds a threshold θ_r are accepted as new nodes, and (old) nodes that lie between two adjacent midpoints whose error is below a smaller threshold θ_c are removed. In our analysis, we take $\theta_c = 0.01\theta_r$. The two end points are always left intact. Note that a judicious choice of the threshold θ_r is important, since a too low value will adaptively create a more dense node set than actually needed. The shape parameters are calculated according to (34), and the interpolation approximation is recomputed using the new node set (= old nodes − removed nodes + new nodes) until the threshold θ_r is satisfied on the entire node set. In other words, the adaptation process follows the adaptive paradigm of solve-estimate-refine/coarsen until a stopping criterion is satisfied.

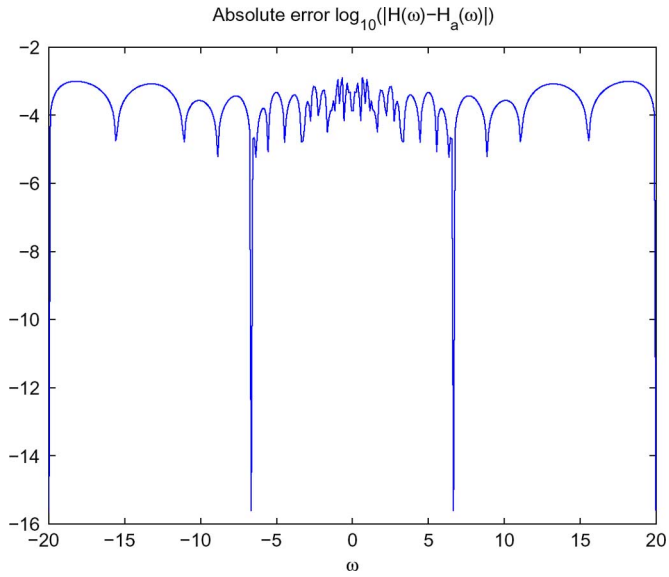

Fig. 2. Logarithmic error for the submarine cable with rational noncausal ARS.

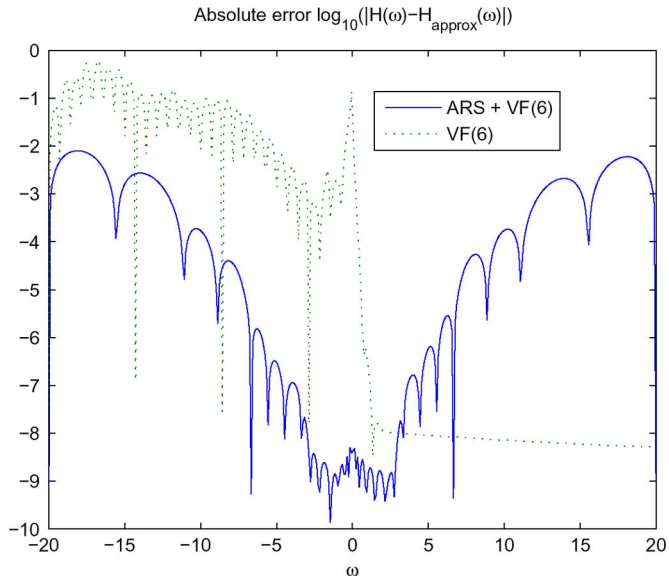

Fig. 3. Logarithmic error for the submarine cable with rational noncausal ARS interfacing nonstable VF.

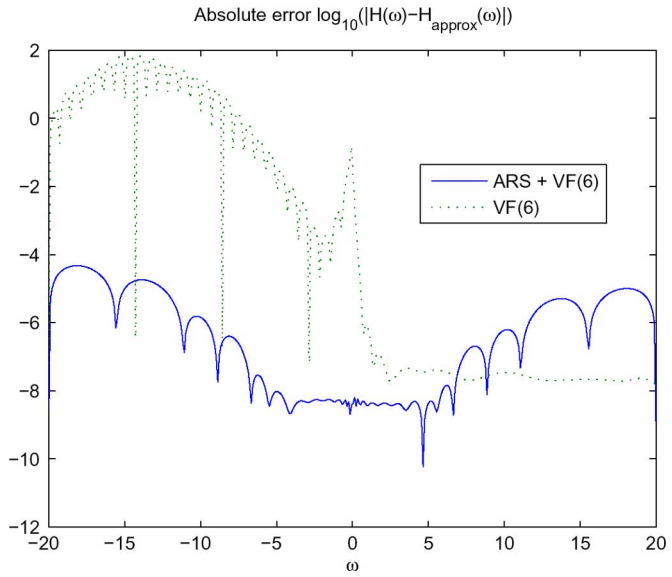

Fig. 4. Logarithmic error for the submarine cable with rational noncausal ARS interfacing stable VF.

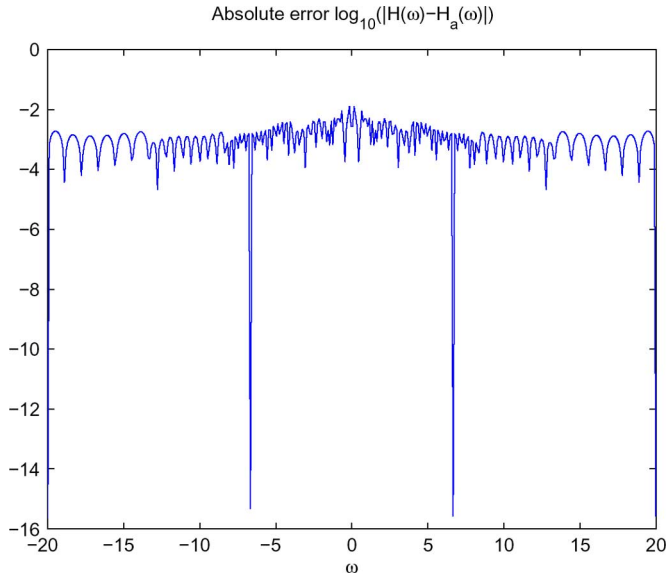

Fig. 5. Logarithmic error for the submarine cable with quasi-rational quasi-causal ARS.

V. Interface With VF

In the VF algorithm [15] (without linear term), one solves the overdetermined system ($N \geq 2M$) with prescribed nodes $\{\omega_n\}$ and starting poles $\{p_m\}$

$$\sum_{m=1}^{M} \frac{c_m}{\omega_n - p_m} - \sum_{m=1}^{M} \frac{H(\omega_n)\tilde{c}_m}{\omega_n - p_m} = H(\omega_n) \qquad n = 1, \ldots, N \tag{36}$$

in a least squares sense for the unknown residues $c_m, \tilde{c}_m$, in order to obtain the rational approximation

$$H_{\text{approx}}(\omega) \approx \frac{\sum_{m=1}^{M} \frac{c_m}{\omega - p_m}}{1 + \sum_{m=1}^{M} \frac{\tilde{c}_m}{\omega - p_m}} = \sum_{m=1}^{M} \frac{\nu_m}{\omega - \tilde{p}_m}. \tag{37}$$

Once the residues $\tilde{c}_m$ obtained, solving the rational equation

$$1 + \sum_{m=1}^{M} \frac{\tilde{c}_m}{\omega - p_m} = 0 \Longrightarrow \tilde{p}_m = \omega_m \tag{38}$$

then defines the mapping (old poles) to (new poles), i.e., $p_m \Rightarrow \tilde{p}_m$. The iterative scheme then proceeds as follows. Starting with some chosen set of poles $\{p_m\}$ we obtain the new set of poles $\{\tilde{p}_m\}$ and so on, until a satisfactory fit is obtained. This of course requires a number r of (hopefully not too much) iterations. The VF algorithm can easily be modified to guarantee causal stability,[2] by pole flipping schemes, which is what we adopt here. More pertinent implementation details can be found in [15] and [16].

The problem with the VF approach is twofold. The first problem is that the sequence of nodes $\{\omega_n\}$ must be given, which implies that some kind of preprocessing sampling was done earlier, most likely equispaced, and hence potentially suboptimal. A second problem is the choice of the starting poles, which is quite heuristic in general. All these problems disappear when one pre-interfaces the VF algorithm with the ARS module, as described previously, the sequence $\{\omega_n\}$ and selectable starting poles are generated automatically by the adaptive method. Since the number of poles generated by the adaptive module is of the order of the number of sampling nodes, we select a limited subset of poles corresponding to the maximum $L_1(\mathbb{R})$ norm, i.e., the poles corresponding to the largest values of

$$\mathcal{S}_j = |d_j| \int_{-\infty}^{\infty} |\phi(c_j(\omega - \omega_j))|\, d\omega = \frac{|d_j|}{c_j} \int_{-\infty}^{\infty} |\phi(\omega)|\, d\omega. \tag{39}$$

In other words, we select the poles corresponding with the largest values of the ratios $|d_j|/c_j$. Interfacing the ARS method with VF therefore provides a fully automated approximation environment. There remains the choice of the interpolation kernel to be used, in our specific case the rational noncausal radial kernel versus the quasi-rational quasi-causal kernel.

VI. Numerical Simulations

In the numerical simulations which follow, we implement three algorithms.

1) The ARS algorithm, with respect to the chosen interpolation kernels.
2) The classic VF algorithm, called VF for comparison purposes, with equispaced nodes and heuristic starting poles as in [15].
3) The preprocessing of VF with ARS, called ARS+VF, which is compared with classic VF.

In all simulations, the number of iterations needed for the VF algorithm are indicated between parentheses in the corresponding figures.

A. Submarine Cable

The transfer function of a submarine cable [18] is given by

$$H(\omega) = e^{-\sqrt{i\omega\tau}}. \tag{40}$$

[2]Note that causal stability of poles in the ω-domain requires $\Re\{ip\} < 0$ or equivalently $\Im p > 0$.

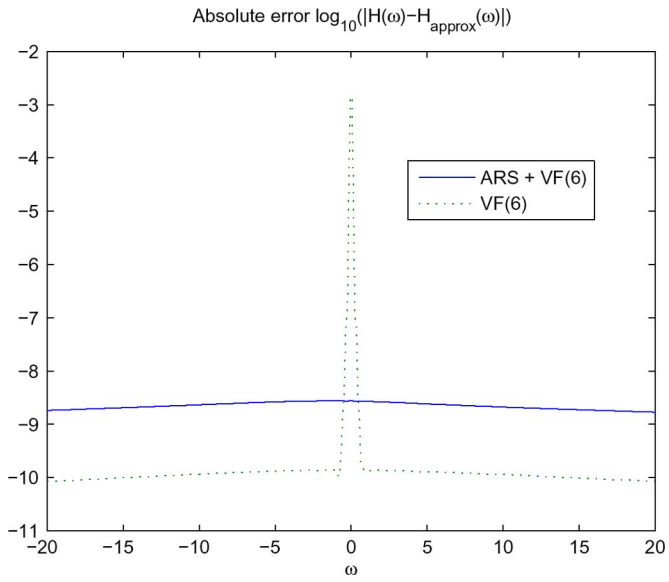

Fig. 6. Logarithmic error for the submarine cable with quasi-rational quasi-causal ARS interfacing nonstable VF.

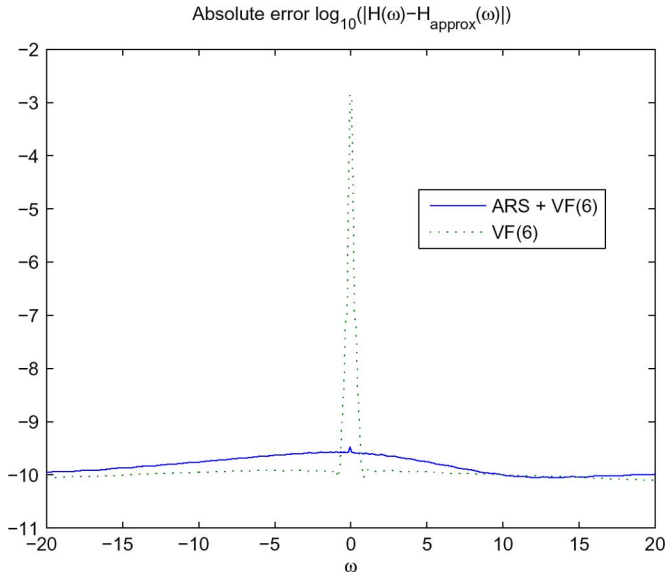

Fig. 7. Logarithmic error for the submarine cable with quasi-rational quasi-causal ARS interfacing stable VF.

This is a causal function with inverse Fourier transform (impulse response)

$$h(t) = \Upsilon(t)\,\frac{e^{-\frac{\tau}{4t}}\sqrt{\tau}}{2\sqrt{\pi}t^{3/2}}. \tag{41}$$

The angular frequency range is $[\omega_1, \omega_N] = [-20, 20]$ and the parameter $\tau = 1$. The causality parameter is $\kappa = 0.01$, corresponding with a causality index $\xi(0.01) = 0.9482$, and the threshold $\theta_r = 0.01$ in the rational noncausal radial case and $\theta_r = 0.02$ in the quasi-rational quasi-causal case. The VF interface is run with 40 poles and $r = 6$ iterations. The error measure utilized is the logarithm of the absolute error, i.e.

$$\mathcal{E}(\omega) = \log_{10}|H(\omega) - H_{\text{approx}}(\omega)|. \tag{42}$$

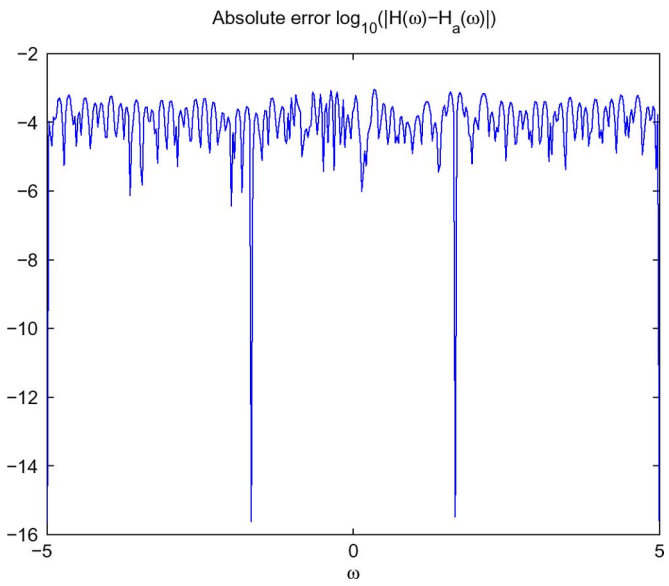

Fig. 8. Logarithmic error for the noncausal example with rational noncausal ARS.

Figs. 2 and 5 show the logarithmic error with rational noncausal, respectively, quasi-rational quasi-causal ARS without VF post-processing. Figs. 3 and 4 indicate that in order to obtain good results, one needs to incorporate the stability requirement in the VF loop. This is because noncausal ARS generates both stable and unstable poles, and hence VF without stability enforcement yields a highly noncausal result which cannot possibly correspond with the inherently causal nature of the submarine cable transfer function. It is also seen that classic VF is generally better than ARS+VF for positive frequencies. Exactly the contrary is seen in Figs. 6 and 7 for quasi-causal ARS: there stability enforcement is not really an issue since VF starts with the stable poles generated by quasi-causal ARS and since the target transfer function is causal. On the other hand, enforcing stability for known causal transfer functions is the correct procedure to follow in general. It should of course be noted that quasi-causal ARS+VF produces better results than noncausal ARS+VF, even with a larger threshold θ_r. It is also seen that classic VF performs well versus ARS+VF, except in the vicinity of $\omega = 0$, where VF cannot resolve the square root branch-point singularity.

B. Noncausal Example

Here we consider the transfer function

$$H(\omega) = \frac{\cos\omega^2 - \sin\omega}{\omega^2 + 1}. \tag{43}$$

Since $H(\omega)$ is real, this is a noncausal function with causality index $\mathcal{C}_1(H) = (1/2)$. Note that the inverse Fourier transform of $H(\omega)$ is not expressible in terms of elementary functions. The angular frequency range is $[\omega_1, \omega_N] = [-5, 5]$. The chosen causality parameter is $\kappa = 0.01$ and the threshold $\theta_r = 0.001$ in the rational noncausal radial case and $\theta_r = 0.01$ in the quasi-rational quasi-causal case. The VF interface is run with 40 poles and $r = 2$ iterations. Figs. 8 and 11 show the logarithmic error with rational noncausal, respectively, quasi-ra-

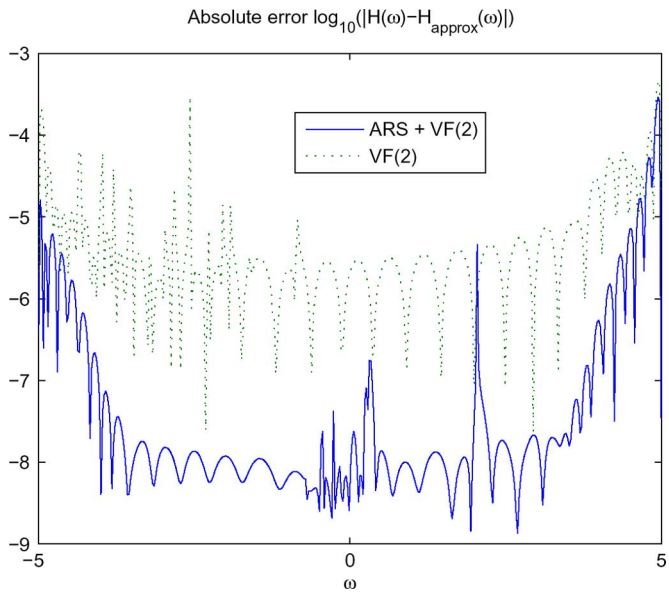

Fig. 9. Logarithmic error for the noncausal example with rational noncausal ARS interfacing nonstable VF.

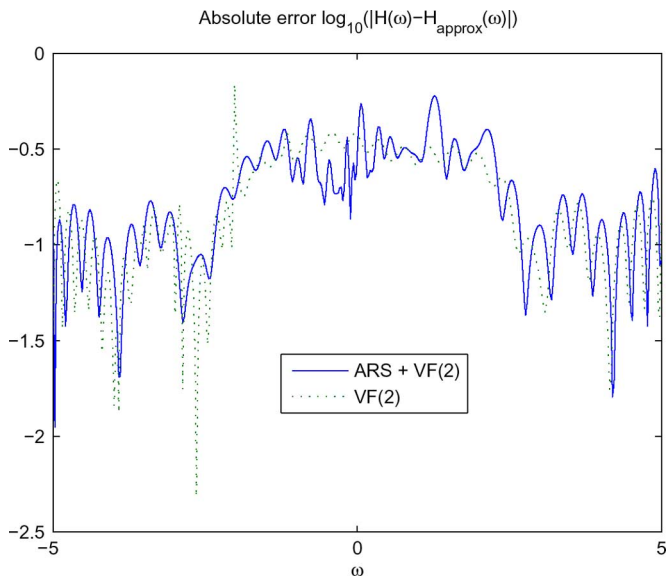

Fig. 10. Logarithmic error for the noncausal example with rational noncausal ARS interfacing stable VF.

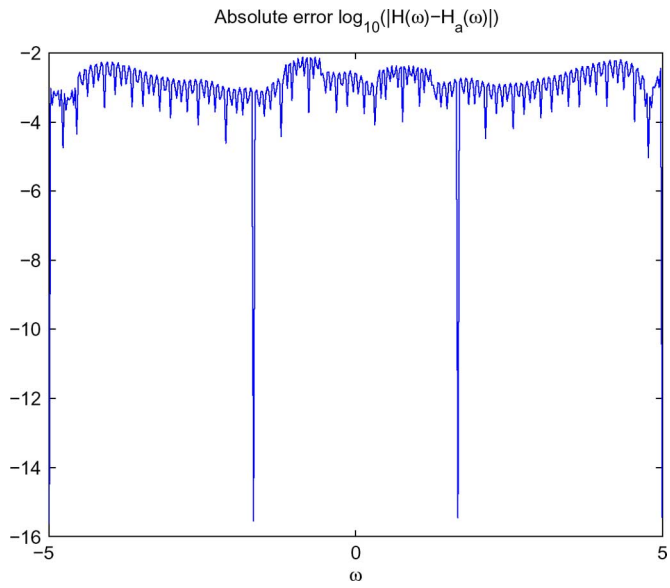

Fig. 11. Logarithmic error for the noncausal example with quasi-rational quasi-causal ARS.

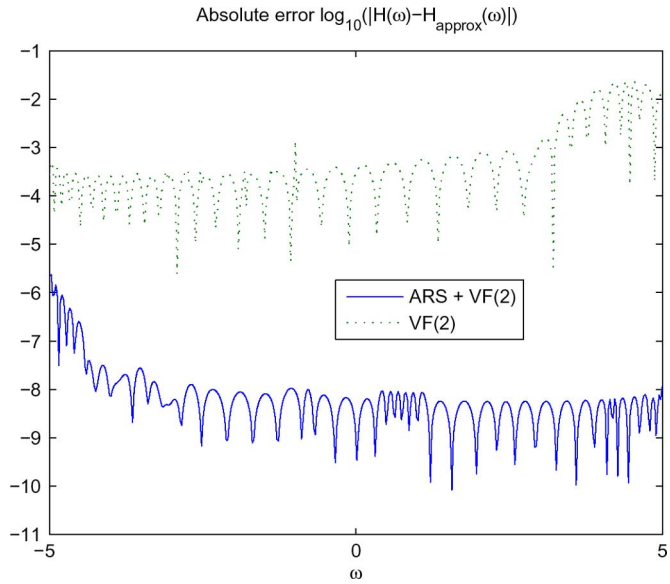

Fig. 12. Logarithmic error for the noncausal example with quasi-rational quasi-causal ARS interfacing nonstable VF.

tional quasi-causal ARS without VF postprocessing. Figs. 9 and 10 indicate that in order to obtain good results, one should certainly not incorporate stability enforcement in the VF loop. This is because the transfer function is strongly noncausal in this example. Exactly the same can be concluded from Figs. 12 and 13. It should of course be noted that quasi-causal ARS+VF produces better results than noncausal ARS+VF, even with a larger threshold θ_r and even for noncausal functions. It is also clear that ARS+VF performs better than classic VF.

C. Real-World Example

As a last example, we consider the frequency response $H(\omega)$ of a microwave bandstop filter. All frequency-domain data samples were simulated with the planar full-wave electromagnetic simulator Agilent EEsof Momentum [19], [20]. Since $H(\omega)$ arises from real-world physical data (but is not necessarily a rational function), it is a causal function. The frequency range is $[\omega_1, \omega_N] = [2, 6]$ (rescaled in GHz for this particular example). A plot of the absolute value $|H(\omega)|$ of the transfer function is shown in Fig. 14. It is seen that the frequency response exhibits high activity in the stopband and near the end of the frequency range. The chosen causality parameter is $\kappa = 0.1$ and the threshold $\theta_r = 0.01$ in the rational noncausal radial case and $\theta_r = 0.03$ in the quasi-rational quasi-causal case. The VF interface is run with 12 poles and $r = 2$ iterations. Figs. 15 and 16 show the logarithmic error with rational noncausal, respectively, quasi-rational quasi-causal ARS with VF postprocessing and stability enforcement. It is seen that the last approach yields the

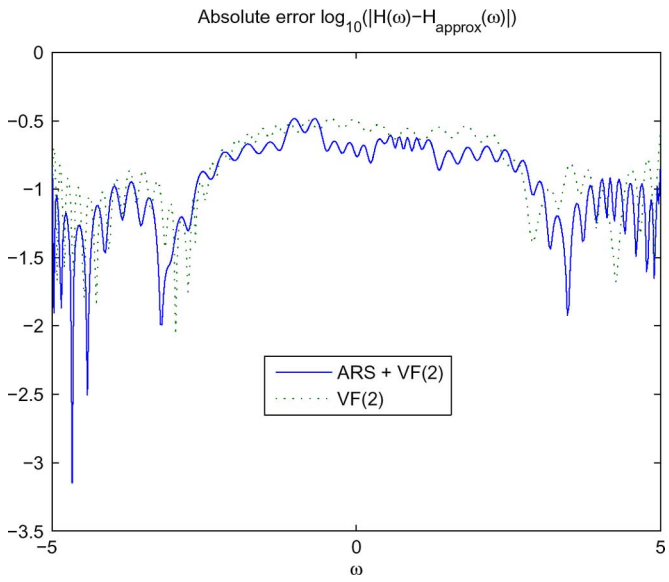

Fig. 13. Logarithmic error for the noncausal example with quasi-rational quasi-causal ARS interfacing stable VF.

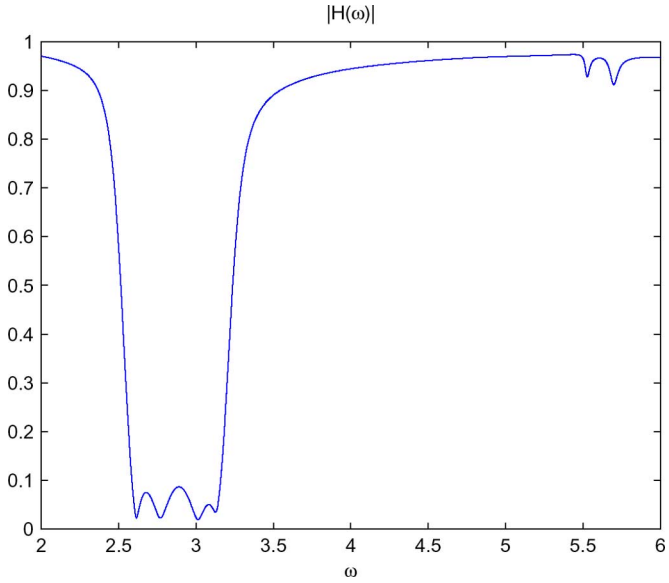

Fig. 14. Absolute value of the transfer function of the real-world microwave bandstop filter.

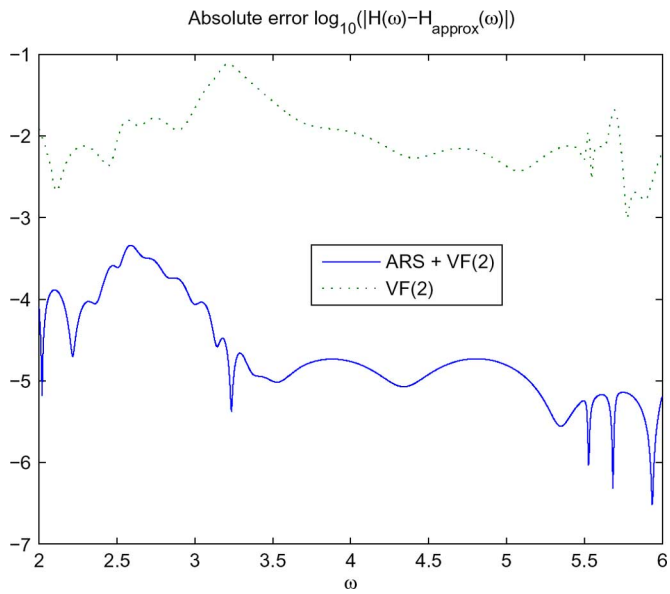

Fig. 15. Logarithmic error for the real-world example with rational noncausal ARS interfacing stable VF.

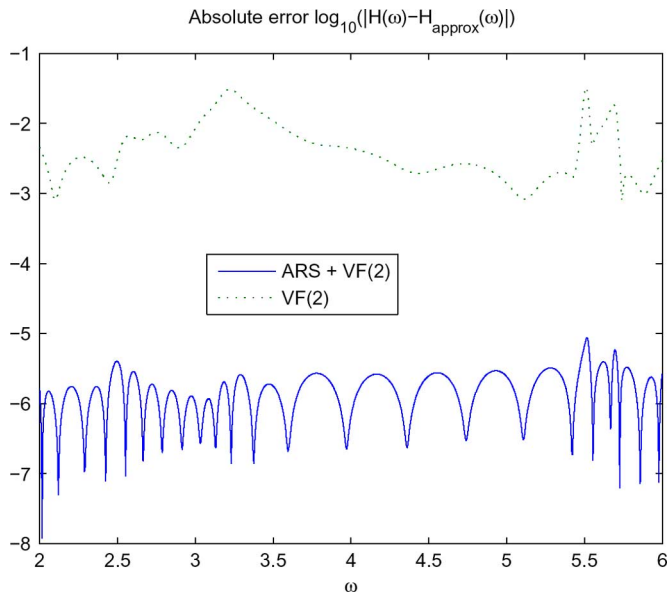

Fig. 16. Logarithmic error for the real-world example with quasi-rational quasi-causal ARS interfacing stable VF.

best results, as could be expected. It is also seen that ARS+VF performs better than classic VF.

VII. Conclusion

We have discussed the translation-invariant interpolation of frequency domain functions by means of Fourier transforms of Pólya frequency functions, which belong to the Bochner class of interpolation kernels. Two pertinent Pólya interpolation kernels were considered, a rational noncausal radial kernel, and a new quasi-rational quasi-causal kernel. For the implementation we have used the fast adaptive ARS interpolation process, which moreover provides an excellent preprocessing interface when used in conjunction with the rational VF algorithm. The result is a composite algorithm, performing the sampling and modelling of the given frequency function in a fully automatic way. An interesting generalization would of course be to extend the algorithm to multivariate quasi-rational radial basis function adaptive interpolation and multivariate VF. Work is currently under way to proceed and (hopefully) succeed in that research direction.

References

[1] M. D. Buhmann, *Radial Basis Functions*. Cambridge, U.K.: Cambridge Univ. Press, 2003.
[2] J. C. Carr, W. R. Fright, and R. K. Beatson, "Surface interpolation with radial basis functions for medical imaging," *IEEE Trans. Med. Imag.*, vol. 16, pp. 96–107, 1997.
[3] T. Poggio and F. Girosi, "Networks for approximation and learning," *Proc. IEEE*, vol. 78, pp. 1481–1497, 1990.
[4] S. Bochner, "Monotone Funktionen, Stieltjes integrale und harmonische analyse," *Math. Ann.*, vol. 108, pp. 378–410, 1933.
[5] T. Blu and M. Unser, "Wavelets, fractals, and radial basis functions," *IEEE Trans. Signal Process.*, vol. 50, no. 3, pp. 543–553, Mar. 2002.

[6] I. J. Schoenberg, "Metric spaces and completely monotone functions," *Ann. Math.*, vol. 39, pp. 811–841, 1938.
[7] F. J. Narcowich, N. Sivakumar, and J. D. Ward, "On condition numbers associated with radial-function interpolation," *J. Math. Anal. Appl.*, vol. 186, no. 2, pp. 457–485, 1994.
[8] I. J. Schoenberg, "On totally positive functions, Laplace integrals and entire functions of the Laguerre-Pólya-Schur type," *Proc. Nat. Acad. Sci. USA*, vol. 33, pp. 11–17, 1947.
[9] I. J. Schoenberg, "On Pólya frequency functions. I. The totally positive functions and their Laplace transforms," *J. d'Analyse Math.*, vol. 1, pp. 331–374, 1951.
[10] I. J. Schoenberg and A. Whitney, "On Pólya frequency functions. III. The positivity of translation determinants with an application to the interpolation problem by spline curves," *Trans. Amer. Math. Soc.*, vol. 74, pp. 246–259, 1953.
[11] T. A. Driscoll and A. Heryudono, "Adaptive residual subsampling methods for radial basis function interpolation and collocation problems," *Comput. Math. Appl.*, vol. 53, pp. 927–939, 2007.
[12] P. Stoica and R. L. Moses, *Introduction to Spectral Analysis*. Englewood Cliffs, NJ: Prentice-Hall, 1997.
[13] A. Cuyt and L. Wuytack, *Nonlinear Methods in Numerical Analysis*. Amsterdam, The Netherlands: North-Holland, 1987.
[14] R. Pintelon, P. Guillaume, Y. Rolain, J. Schoukens, and H. Van Hamme, "Parametric identification of transfer functions in the frequency domain—A survey," *IEEE Trans. Autom. Control*, vol. 39, no. 11, pp. 2245–2260, Nov. 1994.
[15] B. Gustavsen and A. Semlyen, "Rational approximation of frequency domain responses by vector fitting," *IEEE Trans. Power Del.*, vol. 14, no. 3, pp. 1052–1061, Jul. 1999.
[16] W. Hendrickx and T. Dhaene, "A discussion of 'Rational approximation of frequency domain responses by vector fitting'," *IEEE Trans. Power Syst.*, vol. 21, no. 1, pp. 441–443, Feb. 2006.
[17] C. K. Sanathanan and J. Koerner, "Transfer function synthesis as a ratio of two complex polynomials," *IEEE Trans. Autom. Control*, vol. 8, no. 1, pp. 56–58, Jan. 1963.
[18] C. S. Hsu and D. Hou, "Linear approximation of fractional transfer functions of distributed parameter systems," *Electron. Lett.*, vol. 26, no. 15, pp. 1211–1213, Jul. 1990.
[19] Agilent EEsof Comms EDA, ADS Momentum software,. Agilent Technologies, Santa Rosa, CA.
[20] D. Deschrijver and T. Dhaene, "Broadband macromodeling of passive components using orthonormal vector fitting," *Electron. Lett.*, vol. 41, no. 21, pp. 1160–1161, Oct. 2005.

Luc Knockaert (SM'00) received the M.Sc. degree in physical engineering, the M.Sc. degree in telecommunications engineering, and the Ph.D. degree in electrical engineering from Ghent University, Ghent, Belgium, in 1974, 1977, and 1987, respectively.

From 1979 to 1984 and from 1988 to 1995, he was working in North-South cooperation and development projects with the Universities of the Democratic Republic of the Congo and Burundi. He is presently affiliated with the Interdisciplinary Institute for Broadband Technologies (www.ibbt.be) and a professor with the Department of Information Technology, Ghent University. His current interests are the application of linear algebra and adaptive methods in signal estimation, model order reduction, and computational electromagnetics. As author or coauthor, he has contributed to more than 100 international journal and conference publications.

Dr. Knockaert is a member of MAA and SIAM.

Daniël De Zutter (F'00) was born in 1953. He received the M.Sc. degree in electrical engineering from Ghent University, Ghent, Belgium, in 1976. In 1981, he received the Ph.D. degree, and in 1984, completed a thesis leading to a degree equivalent to the French Aggregation or the German Habilitation.

From 1976 to 1984, he was a Research and Teaching Assistant at Ghent University. From 1984 to 1996, he was with the National Fund for Scientific Research of Belgium. He is now a Full Professor of electromagnetics. Most of his earlier scientific work dealt with the electrodynamics of moving media. His research now focuses on all aspects of circuit and electromagnetic modeling of high-speed and high-frequency interconnections, packaging, on-chip interconnect, and on numerical solutions of Maxwell's equations. As author or coauthor, he has contributed to more than 150 international journal papers. Currently, he is the Dean of the Faculty of Engineering, Ghent University.

Tom Dhaene (SM'05) was born in Deinze, Belgium, on June 25, 1966. He received the Ph.D. degree in electrotechnical engineering from Ghent University, Ghent, Belgium, in 1993.

From 1989 to 1993, he was a Research Assistant with the Department of Information Technology, Ghent University, where his research focused on different aspects of full-wave electromagnetic circuit modeling, transient simulation, and time-domain characterization of high-frequency and high-speed interconnections. In 1993, he joined the EDA company Alphabit (now part of Agilent). He was one of the key developers of the planar EM simulator ADS Momentum, ADS Model Composer, and ADS Broadband SPICE. Since 2007, he has been a full professor with the Department of Information Technology, Ghent University. He has authored or coauthored more than 120 peer-reviewed papers and abstracts in international conference proceedings, journals, and books. He holds three U.S. patents.